ELSEVIER

Ceramics International 31 (2005) 507–514

CERAMICS INTERNATIONAL

www.elsevier.com/locate/ceramint

Influence of the dopants on the electrical resistance of hematite-based humidity sensors

J.-M. Tulliani[a,*], P. Bonville[b]

[a]*Politecnico di Torino, Dipartimento di Scienza dei Materiali ed Ingegneria Chimica, Corso Duca degli Abruzzi, 24, 10129 Torino, Italy*
[b]*Commissariat à l'Energie Atomique, Centre d'Etudes de Saclay, Service de Physique de l'Etat Condensé, 91191 Gif-sur-Yvette, France*

Received 24 November 2003; received in revised form 10 May 2004; accepted 24 June 2004
Available online 11 September 2004

Abstract

Humidity sensing properties of α-Fe_2O_3 have been studied after doping with alkali and alkaline earth oxides precursors. Sensors were screen-printed and three different firing temperatures were investigated: 850, 900 and 950 °C. Formation of secondary phases has been investigated by means of ^{57}Fe Mössbauer spectroscopy for K-doped hematite samples and by means of TG–DTA and XRD for all the compositions. Alkali and alkaline earth additions to hematite, except sodium ones, increased the opened porosity as evidenced by mercury porosimetry measurements onto pressed pellets. All the sensors exhibited a strong decrease in resistance as a function of relative humidity, except those doped with barium. Resistances died down over a limited RH range for lithium additions and over a wider range for all the other dopants. However, all the compositions evidenced a scarce sensitivity below 40 and 50% RH.

Keywords: A. Films; C. Electrical properties; D. Ferrites; E. Sensors; Hematite

1. Introduction

Demand for humidity sensors has rapidly grown, from the 70s on, for industrial, medical and home applications such as, for example, paper manufacturing, electronic industry, drugs preparation, respiratory equipments, home dehumidifiers and air conditioners. They could also find extensive use in agriculture for the management of water resources which is one among the big challenges of the third millennium [1]. These sensors have usually to work in the range 10–80% of relative humidity at ambient temperature up to 300–400 °C [2]. At the same time, sensors must be cheap and their response has to be fast and stable with time and temperature. Many polymeric materials have been proposed for this application, due to their low cost, but they cannot withstand high operating temperatures and their stability with ageing is not guaranteed. Ceramic materials, although more expensive, do not suffer these limitations and can thus be coupled with a heater, to periodically regenerate their surface and quickly desorb adsorbed water molecules, after exposure in a high humidity atmospheres. Many oxide ceramic materials have been successfully tested, based for example on TiO_2–SnO_2 [2], SiO_2 [3], $MgFe_2O_4$ [4], $MgCr_2O_4$–TiO_2 [5], $Ba_{0.5}Sr_{0.5}TiO_3$ [6]. Thick film humidity sensor characteristics depend on the bulk and surface properties of the ceramic material: pore size distribution, average particle size and additives. Additions of alkali ions to humidity sensing materials have been widely reported in literature and different hypotheses have been formulated to explain their role [7]. In some cases, alkali additions greatly affect the sensing material microstructure: the percentage of opened porosity increases while the grain size and the average pore size decrease [5]. Alkali ions can also create surface defects or oxygen vacancies and possess high local charge density and strong electrostatic field for the smallest ions such as Li^+, resulting in an increase of adsorption sites for water-vapour adsorption [6,8]. α-Fe_2O_3 pellets [9], as

* Corresponding author. Tel.: +39 011 564 4700; fax: +39 011 564 4665.
E-mail address: jm.tulliani@netcourrier.com (J.-M. Tulliani).

0272-8842/$30.00
doi:10.1016/j.ceramint.2004.06.015

such or doped with SO_4^{2-}, Ti, Sn, Zn or a conducting polymer such as polypyrrole [10–13] have also been successfully tested as humidity sensing materials.

Sensors based on iron oxides belong to the protonic sensors family and their resistance decreases with adsorption of water molecules on their surface [2]. Recently, a screen-printed sensor based on potassium-doped hematite has been patented [14]. Even if some humidity sensors based on α-Fe_2O_3 have been already studied and developed up to a prototype scale, a lack of a systematic study on the electrical response in function of the relative humidity, after doping and as a function of the thermal treatment has been evidenced in the literature.

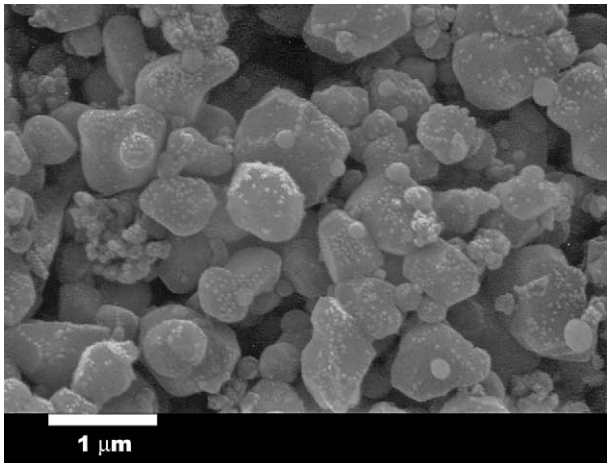

Fig. 1. SEM image of as-received Fe_2O_3 powder.

2. Materials and method

α-Fe_2O_3 powder (Aldrich >99%, particle size distribution lower than 2 μm, Fig. 1) was mixed in ethanol with carbonates (Fluka >99%) used as precursors of the alkali and alkaline-earth oxides listed in Table 1, except for strontium and barium where nitrates were used. After homogenization, in a planetary mill for 1 h and after drying at 80 °C, pellets were uniaxially pressed at 300 MPa and heat treated at 10 °C/min up to 900 °C, under static air, with a soaking time of 1 h at the maximum temperature, in view of Hg-porosimetry measurements. About 75 mg of each doped mixture was also put in an opened platinum crucible for simultaneous thermogravimetric–differential thermal analysis (TG–DTA, Neztsch STA 409) at 10 °C/min up to 900 °C, under static air. XRD (Philips PW 1710, Cu Kα anticathode) were also recorded in the 5–70° 2θ range on the ground pellets after calcination. Additions of K_2CO_3 to α-Fe_2O_3 were studied in details because it is known that potassium has a beneficial effect on the humidity sensing characteristics of hematite: the resistance of the sensor decreases with an increase in the operating temperature and its sensitivity below 50% RH is much better [2]. Therefore, for these doped materials, the influence of the doping agent on the crystal structure of the iron oxide was also investigated by ^{57}Fe Mössbauer spectroscopy.

Sensors were prepared as screen-printed thick layers by using an automatic screen-printer by forcing a viscous paste, called ink, through the openings of a stainless steel screen (325 mesh) by means of a rubber squeegee and, then, by making it to adhere to a substrate after thermal treatment [15]. Inks were made of two components, the active material, i.e. the doped α-Fe_2O_3 powders and an organic vehicle, a mixture of a volatile organic solvent and a resin, which acts as temporary binder for the unfired film and confers the appropriate rheological properties to the paste. In this work the permanent adhesion to the substrate is guaranteed by the presence of the alkali and alkaline-earth dopants. Thick α-Fe_2O_3 films have an area of about 0.4 cm^2 and a thickness of about 30–40 μm. After deposition on α-alumina substrates (0.85 cm × 5.1 cm), samples were dried in air at room temperature prior to be heat treated at 850, 900 or 950 °C for 1 h, with a 2 °C/min heating ramp. Fig. 2 illustrates the sensors structure with platinum (ESL 5545, supplied by Electro-Science Laboratories) interdigitated electrodes (four digits on each electrode, with a 0.4 mm gap (1)) linked to two squared connectors (2) for signal

Table 1
Investigated compositions

Compositions	Ionic radius (pm)	Sensors designation after thermal treatment			
		Ambient	850 °C, 1 h	900 °C, 1 h	950 °C, 1 h
Hematite + 1 wt.% eq. K_2O	K^+: 133	K_1	K_1/850	K_1/900	K_1/950
Hematite + 2 wt.% eq. K_2O	–	K_2	K_2/850	K_2/900	K_2/950
Hematite + 5 wt.% eq. K_2O	–	K_5	K_5/850	K_5/900	K_5/950
Hematite + 10 wt.% eq. K_2O	–	K_{10}	K_{10}/850	K_{10}/900	K_{10}/950
Hematite + 5 wt.% eq. Li_2O	Li^+: 60	Li_5	Li_5/850	Li_5/900	Li_5/950
Hematite + 5 wt.% eq. Na_2O	Na^+: 95	Na_5	Na_5/850	Na_5/900	Na_5/950
Hematite + 5 wt.% eq. Rb_2O	Rb^+: 148	Rb_5	–	Rb_5/900	Rb_5/950
Hematite + 5 wt.% eq. MgO	Mg^{2+}: 65	Mg_5	–	Mg_5/900	–
Hematite + 5 wt.% eq. CaO	Ca^{2+}: 99	Ca_5	Ca_5/850	Ca_5/900	Ca_5/950
Hematite + 5 wt.% eq. SrO	Sr^{2+}: 113	Sr_5	–	Sr_5/900	–
Hematite + 5 wt.% eq. BaO	Ba^{2+}: 135	Ba_5	–	Ba_5/900	–

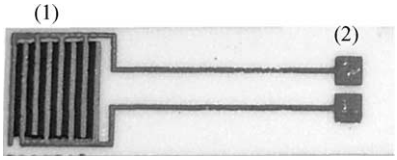

Fig. 2. A screen-printed sensor made of the hematite-doped thick layer with interdigitated Pt electrodes.

collection. Electrodes were screen-printed on previously fired thick layers and, after drying, a second thermal treatment at 850, 900 or 950 °C for 1 h, with a 2 °C/min heating ramp, was performed. Higher heating rates induced diffuse cracking at the interface between metal and ceramic layers.

Platinum was selected as electrode material since it is known [16] that Ag/Pd electrodes, though less expensive, are also less porous than platinum ones, thus leading to a loss of sensibility and stability, longer response time and hysteresis phenomena. The sensors were then designed for further characterisation as shown in Table 1.

Humidity sensors were mounted in a laboratory apparatus for their testing, made of a thermostated chamber in which relative humidity could be varied between 10 and 98% (Fig. 3). In fact, in this device, compressed air (1) was separated into two fluxes: one was dehydrated over a chromatography alumina bed (2) while the second one was directed through two water bubblers (3), generating, respectively, a dry and a humid flow. Two precision microvalves (4) allowed to recombine the two fluxes into one by means of a mixer (5) and to adjust the RH content while keeping constant the testing conditions: a flow rate of 0.1 l/s at 1 m/s. The bubblers, the coils (6) through which the two fluxes passed in, the mixer and the measurement chamber (7) were immersed in a thermostated water bath (8), which in this case operated at 30 °C. A commercial, humidity and temperature probe (9) was used as reference for temperature and RH values (Delta Ohm DO9406, accuracy: ±2.5% in the 5–90% RH range). Each tested sensor (10) was alimented by an external alternating voltage (V = 3.6 V at the rate of 1 kHz) and then constituted a variable resistance of this electrical circuit. The sensor resistance was determined by a calibration curve drawn substituting the sensors, in the circuit, by known resistances. Two sensors of each composition and thermal treatment temperature were tested at each time.

3. Results and discussion

3.1. Potassium additions

The ^{57}Fe Mössbauer absorption measurements were made using a ^{57}Co:Rh source at room temperature on potassium-doped and on non-doped hematite powders heat treated at 850 °C, for 2 h. In all the samples, the isomer shift value (0.2/0.3 mm/s with respect to α-Fe) identified a Fe^{3+} charge state. For non-doped sample the same spectrum was observed (hematite sextet with a hyperfine field of 521 kOe), indicating that thermal treatment had no effect on hematite. In the presence of K_2CO_3 dopant, the samples showed, in addition to basic hematite spectrum, two extra sextets with hyperfine fields of 490 kOe and 441 kOe (Fig. 4). According to literature [17], hematite reacts with K_2CO_3 giving rise to the $KFe_{11}O_{17}$ ferrite, whose spectral signature corresponds to the extra sextets observed in our doped samples. XRD spectra (Fig. 5) confirmed the presence of hematite and of potassium ferrite (JCPDS cards 33-0664 and 25-0651, respectively). The relative $KFe_{11}O_{17}$ content in the doped samples is reported in Table 2; it increases with dopant content (about 10% of ferrite formed for each K_2CO_3 wt.% added), leading to 100% ferrite for a potassium carbonate addition of 10 wt.%.

K^+-β-ferrites with decreasing K^+ content from $K_{1.33}Fe_{11}O_{17}$ down to $KFe_{11}O_{17}$ present an impedance

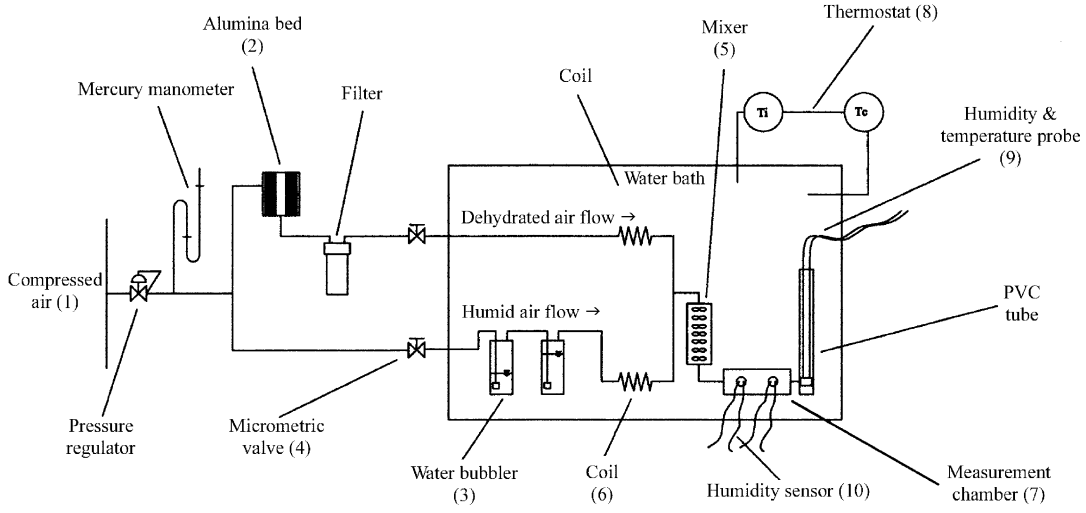

Fig. 3. Scheme of the laboratory apparatus for sensors testing.

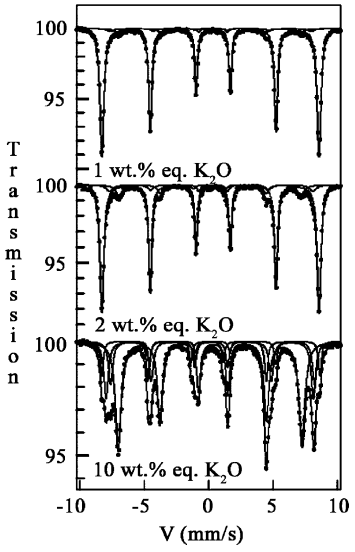

Fig. 4. ^{57}Fe Mossbauer spectra at ambient temperature for K-doped samples.

change under a humid atmosphere which becomes smaller with the increase in the deintercalation, and the humidity characteristics almost disappeared at the $KFe_{11}O_{17}$ composition [18]. The amount of adsorbed water increased with increasing the K^+ ions deintercalated: the more the adsorbed water, the lower the sensitivity. Moreover, the deintercalated samples also presented chemically bound water in the alkali layer [18].

Thick films adhesion onto α-Al_2O_3 substrates was poor for compositions K_1 and K_2, and good for K_5 and K_{10}. Then, Pt electrodes could not be screen-printed on K_1 and K_2 samples without damaging the oxide film. No appreciable variation of average grain size respect to undoped hematite was observed on the surface fracture of a K_5-doped pellet, after 1 h at 900 °C, and only a limited growth was evidenced

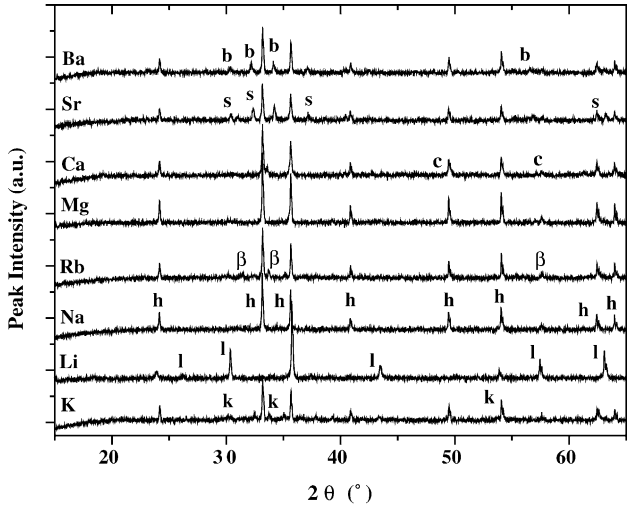

Fig. 5. XRD spectra of doped hematite compositions (h = hematite, k = $KFe_{11}O_{17}$, l = α-$LiFe_5O_8$, β = β''-Fe_2O_3, c = $CaFe_2O_4$, s = $SrFe_{12}O_{19}$, b = $BaFe_{12}O_{19}$).

Table 2
$KFe_{11}O_{17}$ content with respect to hematite for investigated samples

Samples	Ferrite content (wt.%)
K_1/850	9
K_2/850	18.5
K_5/850	45
K_{10}/850	100

on K_{10} pellet. Some geometrical crystals, probably of potassium ferrite, were observed around pores apertures in K_{10}/850 sensors (Fig. 6).

TG curves evidenced the potassium carbonate decomposition between 500 and 744 °C associated with a broad endothermic DTA peak at 674 °C and between 600 and 800 °C with a sharper endothermic peak at 716 °C, respectively, for K_5 and K_{10} compositions. Potassium additions to hematite increased the opened porosity and the mean pore radius (Fig. 7) but did not significantly modify the pore size distribution (Fig. 8), which was very similar between K_5/900 and K_{10}/900 pellets. Sensors resistances died down from 60% RH, for both K_5 and K_{10} specimens, whatever the temperature treatment (Fig. 9).

3.2. Lithium additions

TG curve presented a mass loss of 6.13% from 480 to 680 °C, associated to an endothermic peak at 596 °C, probably due to lithium carbonate decomposition. A second, small endothermic peak at 754 °C was also present on the DTA curve, associated with no mass loss, and this could be due to α-$LiFe_5O_8$ crystallization (JCPDS card 38-0259), as evidenced by XRD spectrum where hematite phase was no more detected after 1-h thermal treatment at 900 °C (Fig. 5). No appreciable variation of average grain size respect to undoped hematite was observed on the surface fracture of the doped pellet, after 1 h at 900 °C. Lithium additions to hematite also led to an increase of the porosity and the mean pore radius (Fig. 7) but did not change the pore size

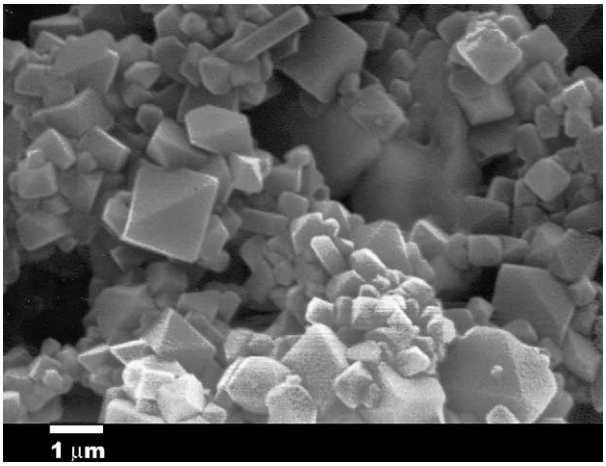

Fig. 6. Crystals found around pores apertures in K_{10}/850 samples.

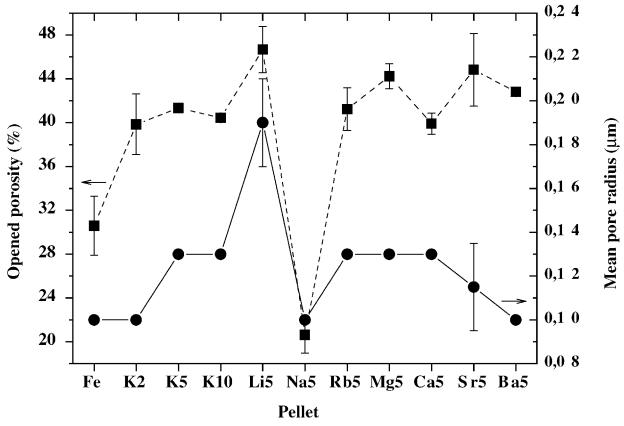

Fig. 7. Total porosity and mean pore radius of the 900 °C heat treated pellets.

distribution. Thick films adhesion onto α-Al_2O_3 substrates was good and sensor resistances decreased continuously from 60% RH, whatever the investigated treatment temperature (Fig. 9). The electrical properties of Li–iron oxide have been studied on thin films treated up to 400 °C [19] and the sensors exhibited a low resistance at low RH and a good response to water vapour. The data suggest that Li^+ promote the conduction mechanism creating preferred sites for the chemisorption of the water molecules [19].

3.3. Sodium additions

TG curves showed a broad mass loss of 7.3% between 400 and 754 °C, associated to two endothermic peaks at 628 and 696 °C, probably due to sodium carbonate decomposition [20]. Only hematite spectrum was identified on XRD spectrum after thermal treatment at 900 °C for 1 h (Fig. 5), though sodium ferrite $Na_2O.1.5Fe_2O_3$ is able to form by decomposing a stoichiometric mixture of Na_2CO_3 and Fe_2O_3 in air at 900 °C for 24 h [21]. A limited increase in average grain size respect to undoped hematite was observed on the surface fracture of the pellets. Sodium doping strongly reduced the total porosity, but did not modify the mean pore radius value (Fig. 7). Mercury porosimetry measurements seemed to evidence a rather limited increase of the pores having a radius below about 0.05 μm respect to undoped α-Fe_2O_3 (Fig. 8). Thick films adhesion onto α-Al_2O_3 substrates was good and sensor resistances decreased continuously from 45% RH to 70% RH, respectively after thermal treatment at 850 and 950 °C (Fig. 9). The slightly different pore size distribution (Fig. 8) could explain the trend of the sensors electrical response: a resistance decrease for lower relative humidity contents respect to K_5/900 composition, according to Kelvin equation where the sensing characteristic of ionic-type humidity sensors is mainly determined by capillary condensation of water in the pores [22]. When the pores are cylindrical with one end close, condensation occurs in all pores with radii up to the

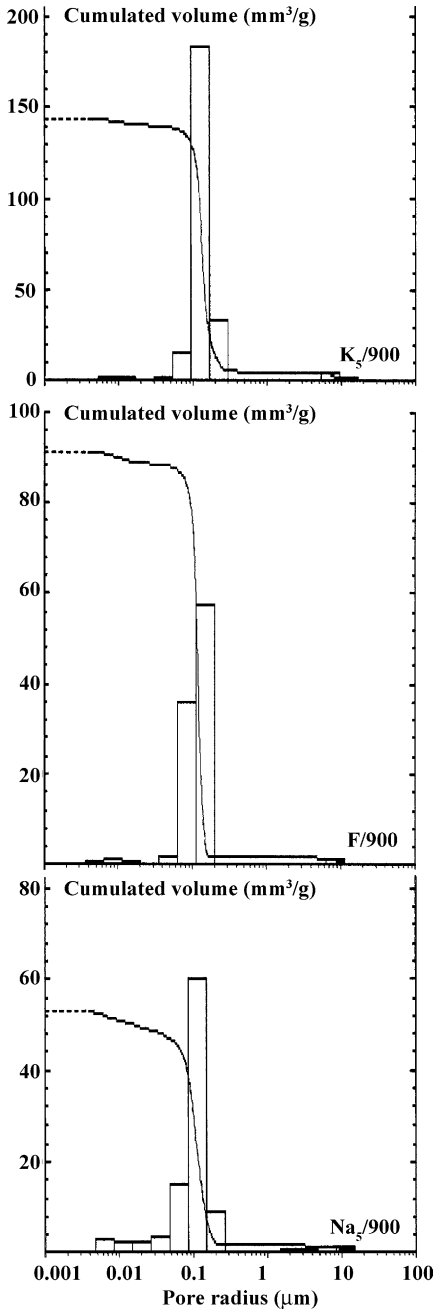

Fig. 8. Pore size distribution in samples Na_5/900, F/900 and K_5/900.

Kelvin radius given by the following Kelvin equation:

$$r_K = \frac{2\gamma M}{\rho RT \ln(P_s/P)} \quad (1)$$

where r_K stands for the Kelvin radius, γ, ρ, and M for the surface tension, density and molecular weight of water respectively, and P and P_s for water vapour pressures in the surrounding environment and at saturation, respectively [22]. Pores of minor dimensions were then first filled with condensed water respect to pores having more important radii, leading to impedance variations for lower relative humidity contents.

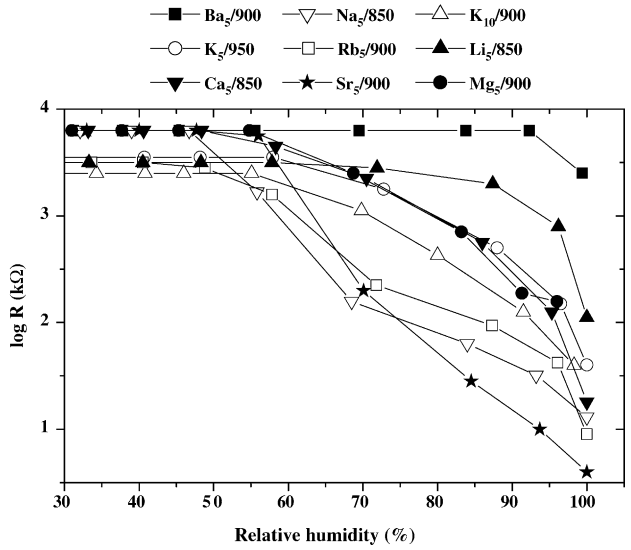

Fig. 9. Sensors resistance at 30 °C in function of RH.

3.4. Rubidium additions

TG curve showed a continuous decrease from 270 °C up to 780 °C associated with a small endothermic peak at 664 °C. XRD spectrum (Fig. 5) showed the presence of hematite and of β″-Fe_2O_3 (JCPDS card 40-1139). No appreciable variation of average grain size respect to undoped hematite was observed on the surface fracture of the doped pellet, after firing. The effect of rubidium additions onto hematite was to increase the total porosity and the mean pore radius (Fig. 7). However, pore size distribution was very close to that of undoped samples. Thick films fired at 850 °C presented a low adhesion onto α-Al_2O_3 substrates and were damaged during electrodes deposition. Sensors heat treated at 900 and 950 °C presented a continuous decrease in the resistance from 40 and 50% RH, respectively (Fig. 9), and this trend could be explained with the same reasons as for sodium-doped thick-films. No data for a comparison are available in the literature concerning sensors based on Rb-doped iron oxide sensors.

3.5. Magnesium additions

For pure magnesite, dissociation peak is at about 630 °C, with a 15 °C/min under static air [23] thus, DTA curve of sample Mg_5 evidenced an endothermic peak at 514 °C, due to magnesium carbonate decomposition into MgO which could then react with Fe_2O_3 from 800 °C to produce magnesium ferrite, $MgFe_2O_4$, reaction which is completed above 1100 °C [24]. XRD spectrum did not evidence any magnesium ferrite formation (Fig. 5), which is favoured by Li_2O doping of MgO and Fe_2O_3 mixed solids, due to the dissolution of Li^+ ions in the lattices of MgO and Fe_2O_3, followed by the creation of one anionic vacancy in each doped solid and then by an increase in the mobility of Mg^{2+} and Fe^{3+} cations [24]. Humidity-sensitive electrical properties of $MgFe_2O_4$ thick films are well-known [25] and depend on the porosity of the film generated by the film thickness, the organic vehicle content and the permanent binder used. Magnesium doping of α-Fe_2O_3 also led to an increase of the total porosity and the mean pore radius of the pellets (Fig. 7). Pore size distribution was not, however, significantly changed respect to pure hematite. Adhesion onto α-Al_2O_3 substrates was poor, then electrodes deposition could only be done on unfired films without damage and sensors were only heat treated at 900 °C for 1 h. The sensors presented a continuous decrease in the resistance from 55% RH (Fig. 9).

3.6. Calcium additions

For pure calcite, dissociation peak is at about 867 °C, with a 15 °C/min under static air [23] thus, DTA curve of sample Ca_5 evidenced an endothermic peak at 742 °C, due to calcium carbonate decomposition into CaO. XRD showed the formation of calcium iron oxide ($CaFe_2O_4$, JCPDS card 32-0168, Fig. 5) after thermal treatment. No significative variation of average grain size respect to undoped hematite was observed on the surface fracture of the doped pellet, after firing. The influence onto the total porosity, the mean pore diameter and the pore size distribution of calcium additions was similar to that of rubidium ones (Fig. 7).

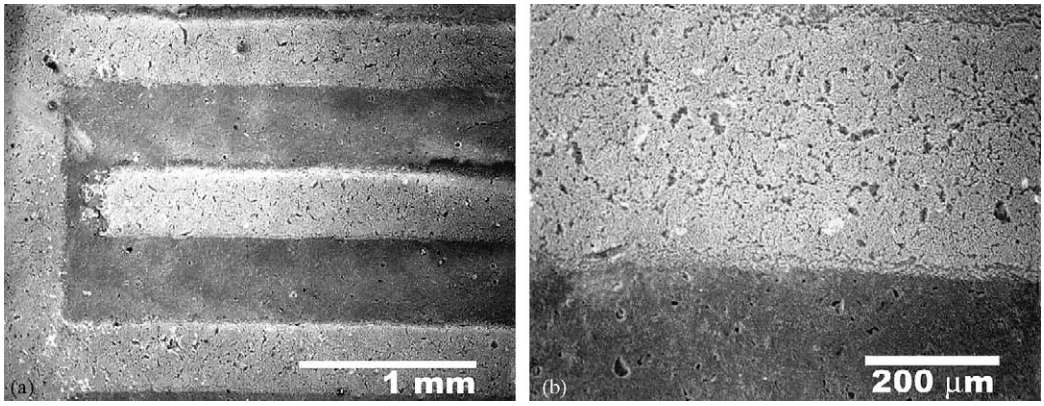

Fig. 10. (a) Strontium-doped sensor with its interdigitated platinum electrode. (b) Detail of the interface between the platinum electrode and the strontium-doped thick film.

All the thick films, whatever the firing temperature, presented a good adhesion onto α-Al_2O_3 substrates. Sensors heat-treated at 850 and at 900 °C presented a continuous decrease in the resistance from 50% and from 55% RH for that heat treated at 950 °C (Fig. 9).

3.7. Strontium additions

DTA curve evidenced an endothermic peak at 580 °C, associated with a mass loss of 3.2%, due to strontium nitrate decomposition. A second small endothermic peak appeared at 808 °C and could be due to $SrFe_{12}O_{19}$ formation, as indicated by XRD spectrum (Fig. 5). Presintered single-phase Sr–ferrite ($SrFe_{12}O_{19}$) is able to form at 1000 °C, from Na_2CO_3, Fe_2O_3 and celestite [26]. No appreciable variation of average grain size respect to undoped hematite was observed on the surface fracture of the doped pellet, after firing. The total porosity and the mean pore radius were higher in strontium-doped samples respect to undoped pellets (Fig. 7), but pore size distribution was very similar. All the thick films, whatever the firing temperature, presented a poor adhesion onto α-Al_2O_3 substrates, then electrodes deposition could only be done on unfired films without damage and sensors were only heat treated at 900 °C for 1 h. The sensors presented a sharp decrease in the resistance only from 55% RH (Fig. 9). SEM observations revealed a limited porosity of the doped-film respect to the metallic electrode (Fig. 10a and b).

3.8. Barium additions

DTA curve evidenced a double endothermic peak at 568 °C and at 596 °C, associated with a mass loss of 1.45% due to barium nitrate decomposition. A second small rather broad endothermic peak was evidenced at 658 °C, probably due to $BaFe_{12}O_{19}$ formation, as demonstrated by XRD spectrum (JCPDS card 39-1433, Fig. 5). No significative variation of average grain size respect to undoped hematite was observed on the surface fracture of the doped pellet, after thermal treatment. The total porosity was higher in Ba_5/900 pellets respect to F/900 ones, but the mean pore radius was the same (Fig. 7). The pore size distribution was very close to K_5/900 pellets (Fig. 8), with no pores below 0.02 mm. These sensors also presented a poor adhesion onto α-Al_2O_3 substrates and platinum electrodes were then deposited on unfired films. After thermal treatment at 900 °C for 1 h, no appreciable resistance decrease was observed in function of humidity variations on four tested sensors (Fig. 9).

All the sensors, except those doped with barium, exhibited a strong decrease in resistance from above 6 MΩ for Na, Mg, Ca, and Sr or from above 3 MΩ for Li, K and Rb additions to several kΩ, when RH was varied. Fig. 9 indicated that all the doped hematite-based sensors were humidity sensitive, except barium–Fe_2O_3, from 40 to 60% RH. There seemed to be no apparent correlation between ionic radii of the dopant cations reported on Table 1 and the resistance values of the sensors (Fig. 9). This could be explained in terms of the evolution of the opened porosity which is increased by doping, except with sodium additions, but the pore size distribution is not radically modified respect to undoped hematite, whatever the cation used.

Multiple sensors testing during setup with K_5 composition have shown a standard deviation of sensors resistance close to 20%, due to screen-printing process: thick films are basically porous after deposition and organic vehicle evaporation during drying step led to a non-uniform porosity distribution within the various sensors. At the beginning of the screen-printing step, all the inks were prepared with the same organic vehicle and temporary binder content, however, corrections were necessary, to obtain screen-printable compositions, in function of the nature of the dopants and their hydrophilic/hydrophobic properties, therefore inks viscosity were not the same, and then the resulting thick films porosity. Fig. 9 also confirmed that on sensors surface water condensed and the conduction mechanism was electrolytic due to interdigitated electrodes above 70% RH for sodium, rubidium and strontium additions, and above 90% RH for potassium, magnesium and calcium doping [27].

4. Conclusions

Some alkali and alkaline-earth-doped hematite humidity sensors have been successfully prepared by screen printing. Different calcinations temperatures have been investigated (850, 900 and 950 °C) when compatible with sensing thick film adhesion onto α-Al_2O_3 substrates. Mössbauer spectroscopy, XRD and DTA curves indicated that some new phases were sometimes formed (ferrites). All the sensors, except those doped with barium, exhibited a strong decrease in resistance over a limited RH range (30%) for lithium additions and over a wider range for all the other compositions. Resistance curves in function of RH seemed to be more dependent on thick films microstructure (porosity) than on ionic radius of the dopants and on the yielded secondary phases: thick films are well-known to be porous and organic vehicle evaporation led to another residual porosity. Inks were all initially prepared with the same vehicle content, but due to the different nature of the dopants (hydrophilic/hydrophobic characteristics) this composition has to be modified to obtain screen printable compositions, thus hindering the effect of the alkali or alkaline earth dopant. Anyway, all the compositions evidenced a lack of response for low humidity atmospheres below 40 and 50 RH%, due to the fact that the dopant cations increased the opened porosity but did not strongly influence the pore size distribution. At the moment, best results were obtained with calcium-doped hematite sensors heat treated at 850 °C and with strontium and potassium based Fe_2O_3 sensors heat treated at 900 °C. Ageing of the doped samples

has now to be verified, as it is known in the literature that alkali cations are not stable under humidified atmospheres and, for example, water vapour attacks sodium β-Al_2O_3 leading to electrical degradation of its properties, depending on the surface texture, the chemical composition and the microstructure [28].

References

[1] R.E. Newnham, Ceramics into the next millennium, Br. Ceram. Trans. 98 (1999) 251–255.

[2] H. Arai, T. Seiyama, Humidity sensors, in: W. Göpel, T.A. Jones, M. Kleitz, I. Lundström, T. Seiyama (Eds.), Sensors. A Comprehensive Survey, 3, VCH, 1991, pp. 982–1012.

[3] F. Uchikawa, K. Shimamoto, Time variability of surface ionic conduction on humidity-sensitive SiO_2 films, Am. Ceram. Soc. Bull. 64 (1985) 1137–1141.

[4] G. Montesperelli, A. Bianco, B. Morten, M. Prudenziati, E. Traversa, The influence of sintering additives on the humidity sensitive electrical properties of $MgFe_2O_4$ thick films, in: G. Gusmano, E. Traversa (Eds.), Proceedings of the 4th Euro-Ceramics, Gruppo Editoriale Faenza Editrice S.p.A., vol. 5, 1995, pp. 467–474.

[5] T.Y. Kim, D.H. Lee, Y.C. Shim, J.U. Bu, S.T. Kim, Effects of alkali oxide additives on the microstructure and humidity sensitivity of $MgCr_2O_4$–TiO_2, Sens. Actuators B (1992) 221–225.

[6] Y.C. Yek, T.Y. Tseng, Electrical properties of K_2O-doped $Ba_{0.5}Sr_{0.5}$–TiO_3 ceramic humidity sensor, IEEE Trans. Compon. Hybrids Manufact. Technol. CHMT-12 (1989) 259–266.

[7] E. Traversa, Ceramic sensors for humidity detection, Sens. Actuators B: Chem. 23 (1995) 135–156.

[8] B.M. Kulwicki, Humidity sensors, J. Am. Ceram. Soc. 74 (4) (1991) 697–708.

[9] C. Cantalini, M. Pelino, Microstructure and humidity-sensitive characteristics of α-Fe_2O_3 ceramic sensor, J. Am. Ceram. Soc. 75 (3) (1992) 546–551.

[10] C. Cantalini, M. Faccio, G. Ferri, M. Pelino, Microstructure and electrical properties of Si-doped α-Fe_2O_3 humidity sensors, Sens. Actuators B 15/16 (1993) 293–298.

[11] F.J. He, T. Yao, B.D. Qu, J.S. Han, A.B. Yu, Gas sensitivity of Zn-doped α-Fe_2O_3 (SO_4^{2-}, Sn, Zn) to carbon monoxide, Sens. Actuators B 40 (1997) 183–186.

[12] P. Chauhan, S. Annapoorni, S.K. Trikha, Humidity-sensing properties of nanocrystalline haematite thin films prepared by sol–gel processing, Thin Solid Films 346 (1999) 266–268.

[13] K. Suri, S. Annapoorni, A.K. Sarkar, R.P. Tandon, Gas and humidity sensors based on iron oxide–polypyrrole nanocomposites, Sens. Actuators B 81 (2002) 277–282.

[14] M. Zucco, A. Negro, L. Montanaro, Sensore di umidità, Italian Patent MI2001A001910 (2001).

[15] P.J. Holmes, R.G. Loasby (Eds.), Handbook of Thick Film Technology, Electrochemical Publication Limited, 1976, pp. 51–73.

[16] W. Qu, Effect of electrodes materials on the sensitive properties of the thick film ceramic humidity sensor, Solid State Ionics 83 (1996) 257–262.

[17] A.T. Howe, G.J. Dudley, J. Solid State Chem. 18 (1976) 149.

[18] S. Ito, M. Washio, I. Makino, N. Koura, K. Akashi, Role of potassium ions in humidity sensitivity of K^+–β ferrite, Solid State Ionics 86/88 (1996) 1005–1011.

[19] G. Neri, A. Bonavita, S. Galvagno, C. Pace, S. Patanè, A. Arena, Humidity sensing properties of Li-iron oxide based thin films, Sens. Actuators B 73 (2001) 89–94.

[20] M.S.R. Swamy, T.P. Prasad, Thermal decomposition of iron(II) sulphate heptahydrate in the presence of alkali metal carbonates, J. Therm. Anal. 25 (1982) 347–354.

[21] S. Hua, G. Cao, Y. Cui, Sodium ferrite $Na_2O1.5Fe_2O_3$ as a high-capacity negative electrode for lithium-ion batteries, J. Power Sources 76 (1) (1998) 112–115.

[22] N. Yamazoe, Y. Shimizu, Humidity sensors: principles and applications, Sens. Actuators 10 (1986) 379–398.

[23] S.St.J. Warne, R.C. Mackenzie, The thermal dissociation of some carbonate materials, J. Therm. Anal. 3 (1971) 49–55.

[24] G.A. El Shobaky, N.R.E. Radwan, F.M. Radwan, Investigation of solid–solid interactions between pure and Li_2O-doped magnesium and ferric oxides, J. Therm. Anal. Cal. 68 (2002) 275–287.

[25] G. Gusmano, G. Montesperelli, P. Nunziante, E. Traversa, M. Prudenziati, Processing of spinel thick films for humidity sensors, in: P. Durán, J.F. Fernández (Eds.), Proceedings of 3rd Euro-Ceramics, Faenza Editrice Iberica, vol. 2, 1993, pp. 449–454.

[26] M. Mozaffari, J. Amighian, Direct use of celestite to prepare $SrFe_{12}O_{19}$ powders, Phys. B Condens. Matter 321 (1–4) (2002) 45–47.

[27] M. Pelino, C. Colella, C. Cantalini, M. Faccio, G. Ferri, A. D'Amico, Microstructure and electrical properties of an α-hematite ceramic humidity sensor, Sens. Actuators B 7 (1992) 464–469.

[28] R.D. Armstrong, D.P. Sellick, A study into the effect of water vapour on sodium β-aluminas, Electrochim. Acta 25 (1980) 1199–1204.